A Method to Correct Steady-State Relative Permeability Measurements for Inhomogeneous Saturation Profiles in One-Dimensional Flow

Guanglei Zhang[1,2] · Sajjad Foroughi[2] · Branko Bijeljic[2] · Martin J. Blunt[2]

Abstract

Traditionally, steady-state relative permeability is calculated from measurements on small rock samples using Darcy's law and assuming a homogenous saturation profile and constant capillary pressure. However, these assumptions are rarely correct as local inhomogeneities exist; furthermore, the wetting phase tends to be retained at the outlet–the so-called capillary end effect. We have introduced a new method that corrects the relative permeabilities, analytically, for an inhomogeneous saturation profile along the flow direction. The only data required are the measured pressure drops for different fractional flow values, an estimate of capillary pressure, and the saturation profiles. An optimization routine is applied to find the range of relative permeability values consistent with the uncertainty in the measured pressure. Assuming a homogenous saturation profile systematically underestimates the relative permeability and this effect is most marked for media where one of the phases is strongly wetting with a noticeable capillary end effect. Relative permeabilities from seven two-phase flow experiments in centimetre-scale samples with different wettability were corrected while reconciling some hitherto apparently contradictory results. We reproduce relative permeabilities of water-wet Bentheimer sandstone that are closer to other measurements in the literature on larger samples than the original analysis. Furthermore, we find that the water relative permeability during waterflooding a carbonate sample with a wide range of pore sizes can be high, due to good connectivity through the microporosity. For mixed-wet media with lower capillary pressure and less variable saturation profiles, the corrections are less significant.

✉ Guanglei Zhang
guanglei.zhang@hebut.edu.cn

[1] School of Civil and Transportation Engineering, Hebei University of Technology, Tianjin 300401, China

[2] Department of Earth Science and Engineering, Imperial College London, London SW7 2BP, UK

1 Introduction

Many natural and industrial processes in fields such as hydrology, petroleum engineering, carbon sequestration, and fuel cell design depend fundamentally on multiphase flow in porous media. Relative permeability and capillary pressure are the two critical parameters needed to quantify multiphase flow (Adler and Brenner 1988; Bear 1988). In recent years, pore-scale X-ray imaging has been combined with special core analysis to determine capillary pressure simultaneously with relative permeability (Gao et al. 2017; Lin et al. 2018; Zou et al. 2018; Zou and Armstrong 2019; Jackson et al. 2020). Small centimetre-sized cylindrical rock samples (cores) are typically used for flow experiments to allow the use of X-ray imaging at a high resolution of a few microns. Both the pore geometry and fluid–fluid interfaces can be visualized and thus pore-scale multiphase flow mechanisms can be quantified. However, the samples are often smaller than those used in traditional core flooding studies without pore-scale imaging.

Some discrepancies have been observed in relative permeability measurements between samples of different size (Qu et al. 2022) as well as between experimental measurements and pore-scale modelling studies (Raeini et al. 2022). Typically, lower relative permeabilities in the pore-scale imaging experiments are observed. The reason for this may be threefold. First, both experiments and predictions may have a large degree of uncertainty (Raeini et al. 2022). Second, local heterogeneity exists, leading to inhomogeneous saturation and the development of capillary pressure gradients. Third, in smaller samples with a diameter of a few millimetres, but lengths of several centimetres, the flow is largely one-dimensional: this means that any inhomogeneity that locally reduces the saturation may significantly restrict flow.

Traditionally, the steady-state relative permeability is calculated using Darcy's law with experimental measurements of pressures and average saturation. This assumes that the saturation profile is homogeneous with the same pressure drop in each phase (the capillary pressure is constant). However, a high pressure gradient will build at a region where the saturation of one phase is low as it will restrict the flow of that phase. Although the average saturation for the whole core may be higher, the overall pressure drop may be dominated by the low saturation regions. As a result, a high pressure drop and a low relative permeability are then assigned to a high average saturation. In this case, the relative permeability is underestimated if a homogeneous saturation profile is assumed.

Furthermore, experimental measurements of relative permeability are affected by the capillary end effect—the capillary pressure vanishes at the outlet, causing retention of the wetting phase (Leverett 1941; Hassker et al. 1944; Osoba et al. 1951). One common method for reducing this effect is to use a flow rate or a high pressure drop in experiments, or to perform the experiment in a larger core (Osoba et al. 1951; Chen and Wood 2001; Gupta and Maloney 2016). However, it is not feasible to perform experiments with high flow rates in many cases, particularly if the aim is to maintain capillary-controlled conditions at the pore scale. To account for the capillary end effect, relative permeabilities are found consistent with the experimental data using numerical techniques, but additional information is often required, such as an independent measurement of capillary pressure as a function of saturation (Virnovsky et al. 1995; Huang and Honarpour 1998; Qadeer et al. 1988; Gupta and Maloney 2016; Zou et al. 2020). Capillary heterogeneity in rocks also leads to inhomogeneous saturation profiles (Krevor et al. 2011). Jackson et al. (2020) developed three-dimensional numerical models to predict the variations in trapping and relative permeability considering the capillary heterogeneity. However, in pore-scale imaging experiments, a long and thin core is typically

used and thus the flow is approximately one-dimensional making a three-dimensional analysis unnecessary.

In this study, we propose an analytical method to correct steady-state relative permeabilities for inhomogeneous saturation profiles including the capillary end effect. This method does not rely on an independent measurement of capillary pressure if capillary pressure can be estimated from interfacial curvature in the images, and does not rely on the use of complex history-matching techniques (Lai and Brandt 1988; Li et al. 2012; Wang et al. 2010; Zhang et al. 2012). To illustrate the approach, seven oil–water two phase flow experiments with pore-scale imaging in the literature with measured saturation profiles and capillary pressures are reanalysed and discussed.

2 Relative Permeability Correction Method for Inhomogeneous Saturation Profiles

In the experiments we study, the fluid flow is upwards, and we assume that the flow is approximately one-dimensional in a long and thin core (see Table 1). The multiphase Darcy's law for one-dimensional vertical two-phase flow is

$$q_1 = -\frac{Kk_{r1}}{\mu_1}\left(\frac{dP_1}{dx} + \rho_1 g\right) \tag{1}$$

$$q_2 = -\frac{Kk_{r2}}{\mu_2}\left(\frac{dP_2}{dx} + \rho_2 g\right) \tag{2}$$

where q is the Darcy velocity, k_r is the relative permeability, μ is the viscosity, P is the pressure, ρ is the density, and g is the gravitational acceleration. The subscripts refer to the two phases, water (phase 1) and a less dense phase 2 (gas or oil). K is the absolute permeability. x is the distance along the flow direction. The capillary pressure P_c is defined as the pressure difference between phases 2 and 1:

$$P_c = P_2 - P_1 \tag{3}$$

Table 1 Pore-scale X-ray imaging with measurement of relative permeability and capillary pressure in steady state two phase flow experiments

Researcher & year	Sample type	Sample size (diameter times length)	Voxel size (µm)
Lin et al. (2018)	Water-wet Bentheimer sandstone	6.1 mm×51.6 mm	3.58
Lin et al. (2019)	Mixed-wet Bentheimer sandstone	6.1 mm×51.6 mm	3.58
Gao et al. (2019)	Water-wet Estaillades carbonate	6.0 mm×51.3 mm	3.58
Lin et al. (2021)	Oil-wet Estaillades carbonate	6.1 mm×43.6 mm	3.58
Alhammadi et al. (2020)	Mixed-wet reservoir carbonate	6.2 mm×50.1 mm	3.57
Gao et al. (2020)	Water-wet reservoir sandstone	6.0 mm×36.0 mm	3.58
Gao et al. (2020)	Mixed-wet reservoir sandstone	6.0 mm×36.0 mm	3.58

By integrating Eqs. (1) and (2) between 0 (the inlet) and the sample length L (the outlet) we find the pressure drop, ΔP, across the sample, which we assume is measured in phase 2 (this will be the case in the experiments we analyse later):

$$\Delta P = \Delta P_2 = \frac{\mu_2 q_2}{K} \int_0^L \frac{1}{k_{r2}(S_1)} dx + \rho_2 g L \tag{4}$$

$$\Delta P = \Delta P_2 = \frac{\mu_1 q_1}{K} \int_0^L \frac{1}{k_{r1}(S_1)} dx + \rho_1 g L + P_c(x = 0) - P_c(x = L) \tag{5}$$

where we account for pressure differences between the phases due to differences in capillary pressure and buoyancy. The capillary pressure at the inlet can be estimated from curvature measurements on the fluid–fluid interfaces or from independent measurements, whereas the capillary pressure at the outlet is assumed to be zero since here both phases are produced with no pressure difference between them. We assume there is a unique relative permeability as a function of saturation: $k_r(S_1)$, which can be defined locally in slice-averages of the image.

$$\Delta P_i = \frac{\mu_2 q_{2,i}}{K} \Delta x \sum_{j=1}^n \frac{1}{k_{r2}(S_1^{i,j})} + \rho_2 g L \tag{6}$$

$$\Delta P_i = \frac{\mu_1 q_{1,i}}{K} \Delta x \sum_{j=1}^n \frac{1}{k_{r1}(S_1^{i,j})} + \rho_1 g L + P_c(x = 0) - P_c(x = L) \tag{7}$$

where we replace the integrals in Eqs. (6) and (7) using the linear sums. Δx is increment of sample length in the images, which is the voxel size in imaging experiments, j is the slice number of the images along the measured saturation profile, and n is the total number of slices. Here i labels the fractional flow: in the experiments we study there are $N=7$ or 8 distinct fractional flow values, f_1, for a waterflood experiment (see Appendix 1)–the first value is a water fractional flow of $0, f_1^1 = 0$, and the last value is $1, f_1^N = 1$.

We determine the initial saturation of phase 1 (water in all the cases we study), S_{1i}, and the residual saturation of phase 2, S_{2r}, from the lowest slice-averaged saturations of phases 1 and 2 respectively measured in these experiments at f_1^1 and f_1^N respectively: we define $k_{r1}^1 = k_{r1}(S_{1i}) = 0$ and $k_{r2}^N = k_{r2}(1 - S_{2r}) = 0$. We divide the measured saturation range from S_{1i} to $1-S_{2r}$ into the same number of increments as the number of fractional flows in each experiment, N. Hence we describe the relative permeabilities of phases 1 and 2 using seven or eight unknowns at discrete points $k_{r1,i}$ and $k_{r2,i}$. The saturations for each relative permeability value are the average saturations at each fractional flow—that is the same saturations as for the uncorrected data. We use linear interpolation to define relative permeability values at any saturation between these discrete points as a weighted linear sum of the unknowns.

To determine the relative permeability values, we use differential evolution which is a stochastic optimization technique to minimize the errors between the pressure gradient integrated along the measured saturation profile and the experimentally measured pressure drop. Differential evaluation (DE) is a stochastic population-based optimization algorithm introduced by Storn (1996). This metaheuristic method can search a

large space of candidate solutions. This method makes a few assumptions about problem being optimized and does not use the gradient of the problem being optimized which means does not require the optimization problem to be differentiable. The DE algorithm starts with a population of candidate solutions (called agents). These agents are moved around in the search-space using simple mathematical formulae to combine the existing agents from the population. If the new agent is an improvement, then it is accepted and forms part of the population, otherwise it is simply discarded. The process is repeated until a satisfactory solution is found.

The objective function is:

$$\min \left| \frac{\Delta P_i^{\text{calculation}} - \Delta P_i^{\text{experiment}}}{\Delta P_i^{\text{experiment}}} \right| \tag{8}$$

where k_{r1} and k_{r2} are the adjusted parameters. The solution is constrained to ensure that the relative permeabilities are monotonic:

$$k_{r1,i+1} > k_{r1,i} \tag{9}$$

$$k_{r2,i+1} < k_{r2,i} \tag{10}$$

$$0 < k_{r1,i} < 1 \text{ and } 0 < k_{r2,i} < 1 \tag{11}$$

The monotonicity constraints (Eqs. 9 and 10) are implemented using a penalty function. The objective function (Eq. 8) was minimized to have two characteristics. The optimized relative permeabilities should give less error than the error based on relative permeabilities obtained from an assumed uniform saturation profile. Also, the optimized relative permeabilities should predict pressure differences within the range of uncertainty of the measurements, which we assume to be 20%. This uncertainty in the experimental measurement leads to an uncertainty in the optimization and all the solutions with the above characteristics will be accepted. We find a range of relative permeability consistent with the uncertainty in the experimental measurements.

3 Results and Discussion

Relative permeabilities from seven two-phase flow experiments obtained using pore-scale imaging from our research group with the results available in the literature were corrected for inhomogeneous saturation profiles using the method developed here. These seven two-phase flow experiments are the only publicly available datasets with measured pressure drops, saturation profile and capillary pressure combined. The pressure drops, saturation profiles along the length of the samples, and capillary pressures for each fractional flow are available in these experiments, see Appendix 1. These seven datasets include water-wet and mixed-wet Bentheimer sandstones, water-wet and oil-wet Estaillades carbonates, a mixed-wet reservoir carbonate, and a reservoir sandstone with the same geometry under two wettability conditions (Table 1). In these experiments phase 1 is water (or brine) and phase 2 is oil.

3.1 Bentheimer Sandstone

Bentheimer sandstone comes from shallow marine formation deposited during the Lower Cretaceous, which forms a reservoir for oil found on the border between the Netherlands and Germany (Peksa et al. 2015). Bentheimer is considered as an ideal rock for reservoir studies because of its lateral continuity and homogeneous block-scale nature. Bentheimer has been used as a benchmark for multiphase flow experiments (Øren et al. 1998; Herring et al. 2013; Alizadeh and Piri 2014; Gao et al. 2017; Lin et al. 2018, 2019). Gao et al. (2017) and Lin et al. (2018) conducted steady-state two-phase flow experiments with co-injection of water and oil into water-wet Bentheimer samples. Lin et al. (2019) also conducted steady-state two-phase flow experiments on a mixed-wet Bentheimer sample. The measured saturation profiles and relative permeabilities before and after correction for the measured inhomogeneous saturation profiles can be found in Figs. 1 and 2.

The originally reported relative permeabilities are lower than those of the previously published for larger, full-core experiments under water-wet conditions (Øren et al. 1998; Alizadeh and Piri 2014). Lin et al. (2018) corrected the water relative permeabilities by considering a constant gradient in capillary pressure which did lead to an increase in the estimated water relative permeability, but it was still lower than in the other experiments. Qu et al. (2022) measured the rate of spontaneous imbibition on samples from the same block of stone used by Lin et al. (2018). Using a semi-analytical solution for the imbibition rate, they estimated a water relative permeability that was consistent with previous measurements, but higher than reported by Lin et al. (2018). This discrepancy in measurements on a homogeneous sandstone, although just within the reported experimental uncertainty, was concerning and raised the possibility that measurements of macroscopic properties on the small samples used for pore-scale imaging might not be as accurate as those on larger cores.

In Fig. 1 it is evident that in the water-wet case, not only there is a noticeable gradient in saturation but also the profiles themselves show large fluctuations. Where the water saturation is locally small, flow is restricted and the pressure gradient is large: associating a relative permeability, consistent with the measured pressure drop, to the average saturation will tend to underestimate the true value. For the mixed-wet sample, although small fluctuations are also present, they are less significant, while the capillary pressure is very low, and so little correction in relative permeability is needed. This
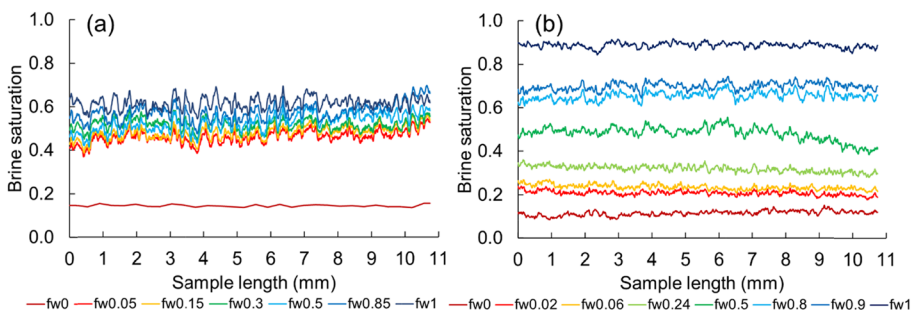

Fig. 1 Brine (phase 1) saturation profiles for different fractional flows in the middle part of the sample measured in the experiments, which is rescaled to the full length of the sample for the analysis in this paper. **a** Water-wet Bentheimer sandstone (Lin et al. 2018); **b** mixed-wet Bentheimer sandstone (Lin et al. 2019)
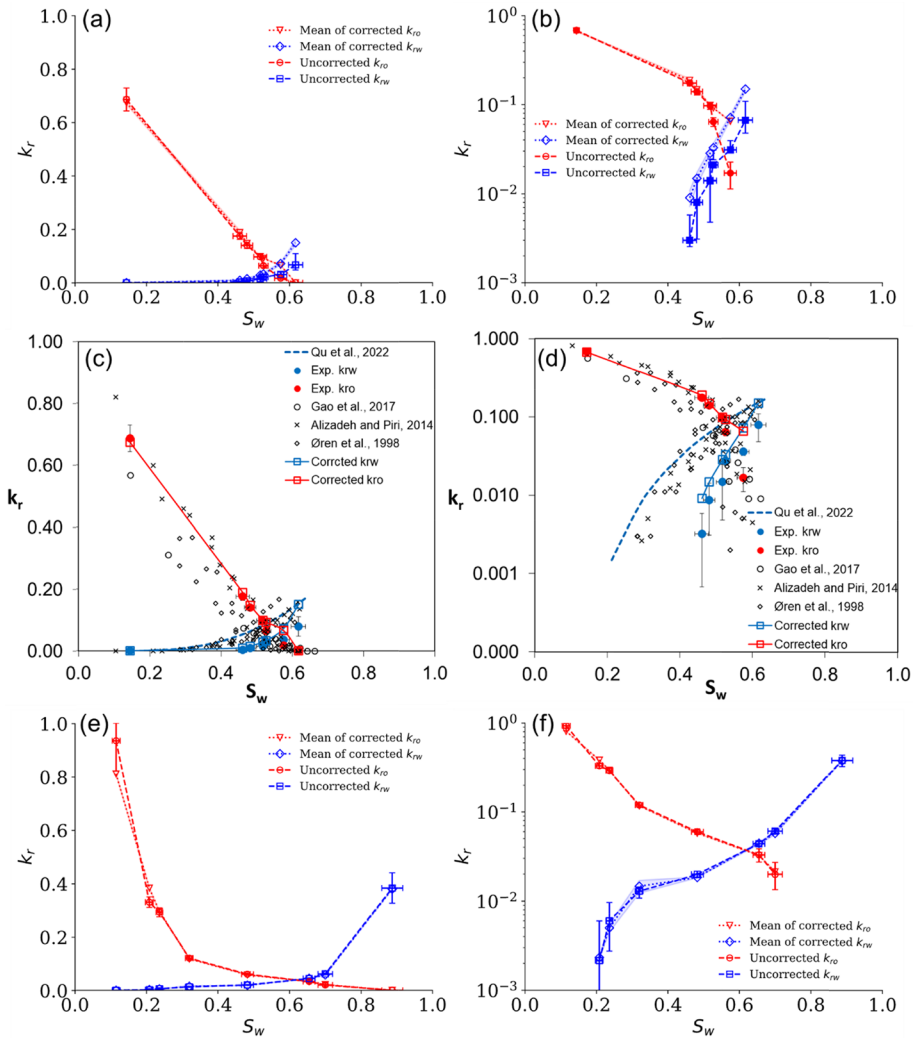
Fig. 2 Relative permeabilities for phase 1 (water/brine, blue) and phase 2 (oil or gas, red) with and without the inhomogeneous saturation profile correction shown on a linear axis (left) and on a semi-logarithmic axis (right): **a** and **b** water-wet Bentheimer sandstone (Lin et al. 2018); **c** and **d** water-wet Bentheimer sandstone (Lin et al. 2018) compared to the pore-scale imaging experimental data by Gao et al. (2017), and traditional core-flood data by Øren et al. (1998) and Alizadeh and Piri (2014), and from spontaneous imbibition measurements by Qu et al. (2022); **e** and **f** mixed-wet Bentheimer sandstone (Lin et al. 2019). The error bars indicate the uncertainty in the measurement of saturation and pressure drop, while the shaded areas represent the uncertainty of the corrected relative permeabilities after optimization

is confirmed in Fig. 2, where the water (phase 1) relative permeabilities in water-wet Bentheimer systematically increase after our correction. The end point values are close to those of the other experiments in the literature: the apparent discrepancy is resolved through a proper accounting for variations in the saturation profile.

For the mixed-wet Bentheimer, the relative permeabilities show little change after correction. This is reassuring, and adds confidence to the results, which indicate potentially favourable waterflood recovery in this case.

3.2 Estaillades and Reservoir Carbonates

Three carbonates, namely water-wet Estaillades, oil-wet Estaillades and a mixed-wet reservoir carbonate are selected in our study. Estaillades carbonate is a bioclastic limestone, which contains 99% calcite, quarried near the town of the Oppède, south of France. It has a complex sub-micron pore space with a large range of pore sizes, which is a benchmark microporous carbonate for relative permeability analysis. The reservoir sample comes from a producing oil field in the Middle East; wettability was restored by placing the rock in contact with crude oil from the same reservoir for several weeks at high temperature and pressure (Alhammadi et al. 2020). Figure 3 shows the measured saturation profiles in the experiments while Fig. 4 compares the relative permeability results with and without correction.

Both oil and water relative permeability increase significantly after correction as there is a clear saturation gradient in the water-wet Estaillades carbonate experiments with significant local fluctuations, Fig. 3a. Estaillades carbonate has a large fraction of
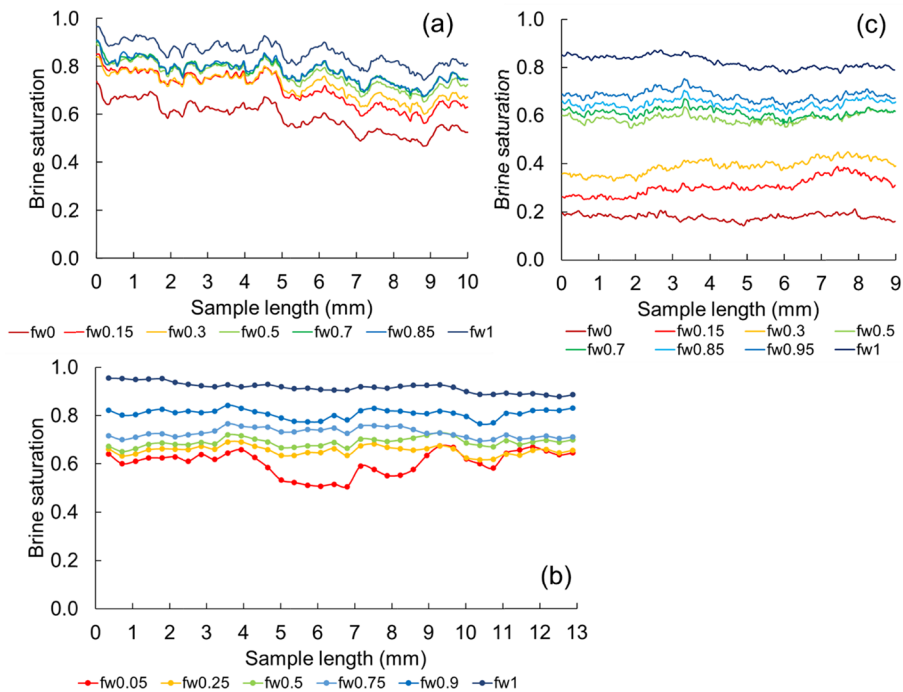

Fig. 3 Brine (phase 1) saturation profiles in the middle part of the sample measured in the experiments, rescaled to the full length for the analysis in this paper. **a** Water-wet Estaillades carbonate (Gao et al. 2019); **b** oil-wet Estaillades carbonate, where 100 image slices are averaged for each point, representing approximately 0.36 mm in length along the sample (Lin et al. 2021); **c** mixed-wet reservoir carbonate (Alhammadi et al. 2020)
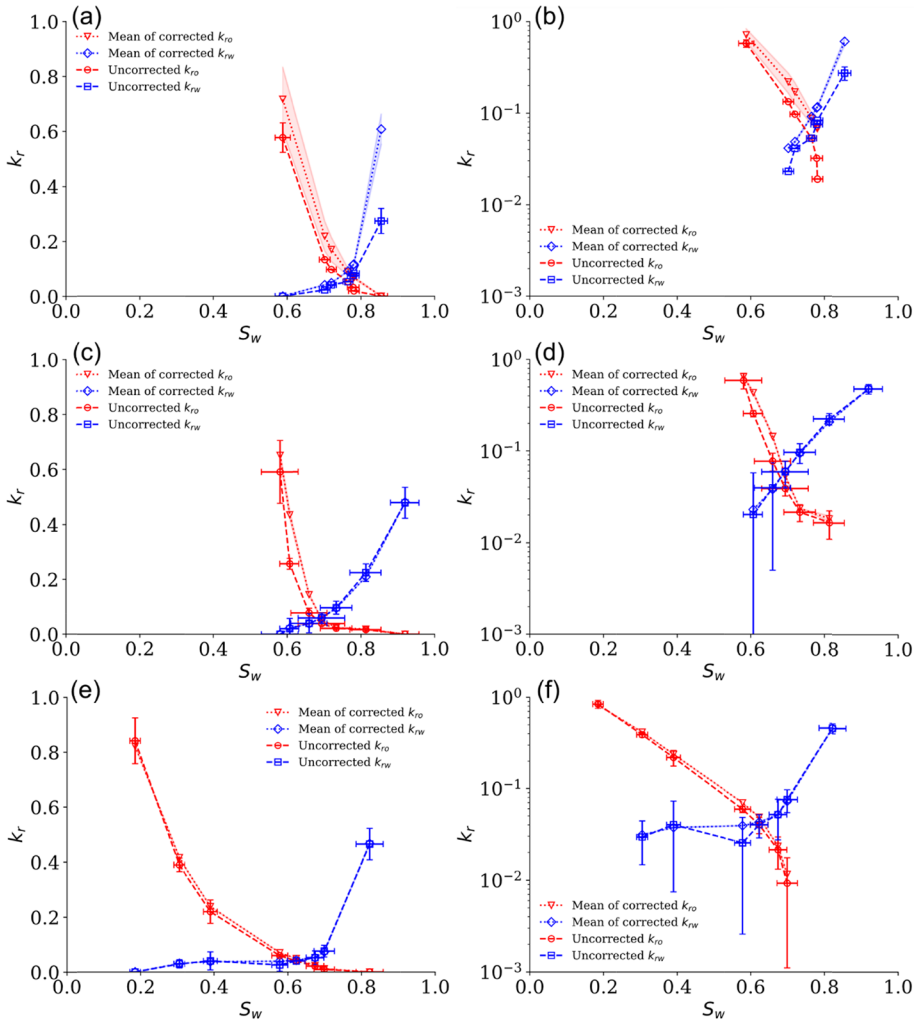
Fig. 4 Relative permeabilities for water (brine, phase 1, blue) and oil (phase 2, red) with and without the inhomogeneous saturation profile correction shown on a linear axis (left) and on a semi-logarithmic axis (right): **a** and **b** water-wet Estaillades carbonate (Gao et al. 2019); **c** and **d** oil-wet Estaillades carbonate (Lin et al. 2021); **e** and **f** mixed-wet reservoir carbonate (Alhammadi et al. 2020). The error bars indicate the uncertainty of the measurements of saturation and pressure drop, while the shaded areas represent the uncertainty of the corrected oil and water relative permeability after optimization

macropores that are connected through sub-resolution microporosity with a high initial water saturation at the beginning of waterflooding. Compared to the Bentheimer sandstone results shown in Fig. 2, although there is trapping of oil in macropores, sub-resolution microporosity provides good connectivity leading to a much higher end-point water relative permeability even in this water-wet sample.

In oil-wet Estaillades carbonate, the saturation profiles are smoother with no obvious gradient: the oil relative permeabilities increase whereas there are no obvious changes in the water relative permeabilities after correction.

The reservoir sample shows a relatively smooth saturation profile (Fig. 3c) and the correction only makes small adjustments to the oil and water relative permeabilities. This confirms the validity of the original analysis (Alhammadi et al. 2020) and the suggestion that mixed-wet media can lead to high recoveries in waterflooding.

3.3 Reservoir Sandstone Under Two Wettability Conditions

Gao et al. (2020) simultaneously measured relative permeability and capillary pressure on the same reservoir sandstone sample under water-wet and mixed-wet conditions, before and after exposing the rock to a crude oil at high temperature. Figure 5 shows the measured saturation profiles for each fractional flow for both experiments, while Fig. 6 compares the relative permeability results before and after correction. Raeini et al. (2022) used a generalized pore network model to predict capillary pressure and relative permeability for this case. The modelling results showed a reasonable match with the measurements within the uncertainty of the experiments. However, the presented experimental water relative permeabilities were lower than the predictions. Here, we see an increase in the relative permeability values after correction, which are then closer to the modelling results (Raeini et al. 2022). Here the increase in relative permeability values
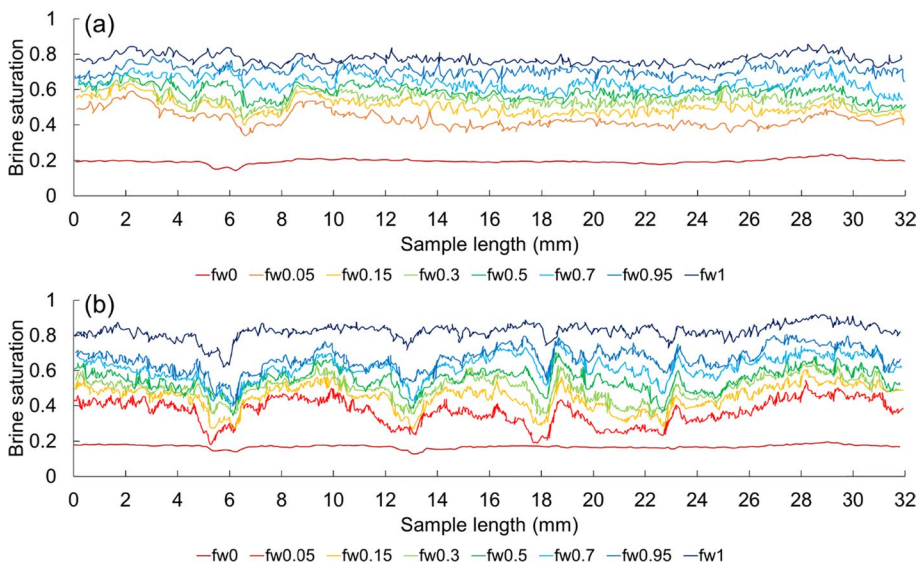

Fig. 5 Brine saturation profiles along the sample measured in experiments. **a** Water-wet reservoir sandstone (Gao et al. 2020); **b** mixed-wet reservoir sandstone (Gao et al. 2020)
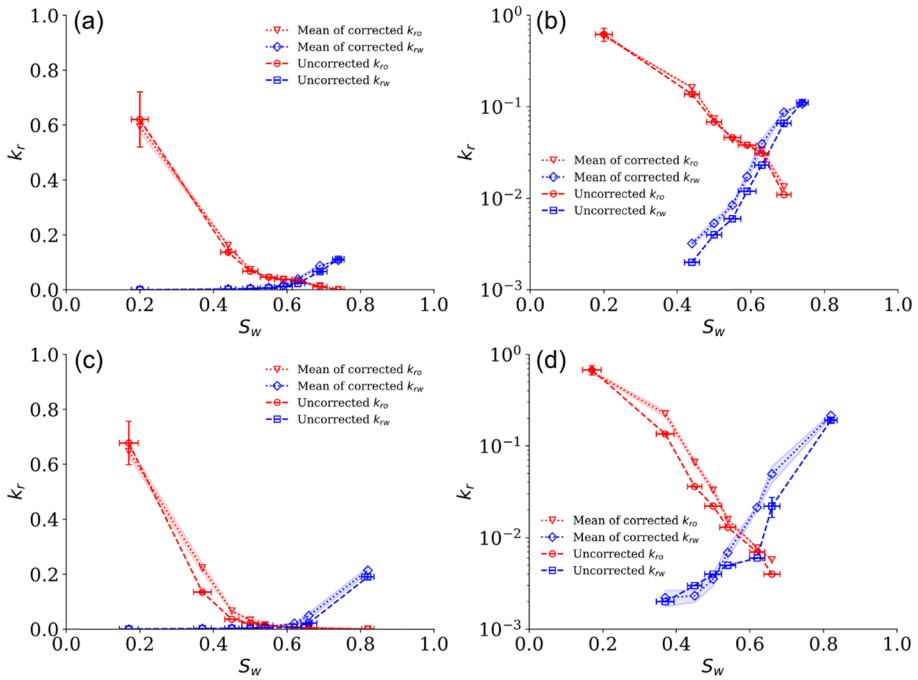
Fig. 6 Relative permeabilities for oil (red) and water (blue) with and without the inhomogeneous saturation profile correction shown on a linear axis (left) and on a semi-logarithmic axis (right): **a** and **b** water-wet reservoir sandstone (Gao et al. 2020); **c** and **d** mixed-wet reservoir sandstone (Gao et al. 2020). The error bars indicate the uncertainty of the measured saturation and pressure drop, while the shaded areas represent the uncertainty of the corrected oil and water relative permeability after optimization

is more obvious in the mixed-wet experiment, as more heterogeneous saturation profiles are observed compared to the water-wet case.

4 Conclusions

We have introduced a novel method to correct for inhomogeneous saturation profiles and the so-called capillary end effect in steady-state measurements of relative permeability. This method only requires pressure drops, saturation profiles and capillary pressures for each fractional flow. It assumes one-dimensional flow along the sample and that the relative permeability can be written as a single function of saturation. The method does not require additional measurements from independent techniques if the capillary pressure can be estimated from the interfacial curvature in the pore-space images. Where there are significant variations in the saturation profile, our methodology leads to larger estimates of relative permeability than would be assumed assigning a value to the average saturation.

We applied this methodology to seven experimental datasets in the literature. We resolved an apparent discrepancy in results for water-wet Bentheimer sandstone between pore-scale imaging experiments and the results of traditional core floods, as well as measurements of the rate of spontaneous imbibition. For a carbonate sample with a wide range of pore size, we demonstrated that the water relative permeability can be high, even under water-wet conditions, due to good connectivity through microporosity. For two of the mixed-wet media studied, the measured saturation profile showed only small fluctuations and the capillary pressure was low, and hence the correction to relative permeability was insignificant. This strengthens the original conclusion that mixed-wet conditions may lead to favourable local displacement efficiency in waterflooding.

Overall, we suggest applying this correction to experiments where the flow is largely one-dimensional and where the saturation profile is measured.

Appendix 1: Saturation, pressure, and relative permeability with and without correction in oil–water two phase flow in seven experiments

See Tables 2, 3, 4, 5, 6, 7 and 8.

Table 2 Water-wet Bentheimer sandstone (Lin et al. 2018)

f_w	S_w	ΔP/kPa	P_c/kPa	Experimental k_{rw}	Experimental k_{ro}	Corrected k_{rw}	Corrected k_{ro}
0	0.144	1.75	0	0	0.686	0	0.674
0.05	0.461	6.51	2.56	0.003	0.175	0.009	0.188
0.15	0.481	7.27	2.54	0.009	0.140	0.015	0.148
0.3	0.518	8.65	2.39	0.015	0.097	0.028	0.098
0.5	0.527	9.42	2.30	0.027	0.064	0.033	0.092
0.85	0.575	10.8	2.37	0.036	0.017	0.072	0.065
1	0.617	5.94	2.22	0.079	0	0.150	0

Table 3 Mixed-wet Bentheimer sandstone (Lin et al. 2019)

f_w	S_w	ΔP/kPa	P_c/kPa	Experimental k_{rw}	Experimental k_{ro}	Corrected k_{rw}	Corrected k_{ro}
0	0.115	1.31	0	0	0.934	0	0.810
0.02	0.208	3.64	0	0.002	0.330	0.002	0.383
0.06	0.236	3.95	-0.311	0.006	0.292	0.005	0.295
0.24	0.320	7.74	-0.26	0.013	0.120	0.015	0.118
0.5	0.482	10.14	-0.28	0.020	0.060	0.019	0.058
0.8	0.655	7.42	-0.26	0.044	0.033	0.045	0.033
0.9	0.700	6.02	-0.15	0.061	0.020	0.058	0.021
1	0.887	1.07	0	0.383	0	0.379	0

Table 4 Water-wet Estaillades carbonate (Gao et al. 2019)

f_w	S_w	ΔP/kPa	Experimental k_{rw}	Experimental k_{ro}	Corrected k_{rw}	Corrected k_{ro}
0	0.588	289.99	0	0.577	0	0.717
0.15	0.702	1068.42	0.023	0.133	0.041	0.219
0.3	0.72	1204.41	0.041	0.097	0.048	0.170
0.5	0.765	1538.00	0.053	0.053	0.091	0.088
0.7	0.779	1540.52	0.075	0.032	0.114	0.069
0.85	0.781	1680.01	0.083	0.019	0.117	0.068
1	0.855	600.01	0.274	0	0.608	0

Table 5 Oil-wet Estaillades carbonate (Lin et al. 2021)

f_w	S_w	ΔP/kPa	P_c/kPa	Experimental k_{rw}	Experimental k_{ro}	Corrected k_{rw}	Corrected k_{ro}
0	0.58	5.37	0	0	0.590	0	0.651
0.05	0.61	11.69	− 1.31	0.020	0.257	0.023	0.434
0.25	0.66	30.48	− 1.67	0.040	0.077	0.038	0.144
0.5	0.69	40.62	− 1.72	0.059	0.039	0.060	0.053
0.75	0.73	36.87	− 1.98	0.097	0.021	0.094	0.024
0.9	0.81	19.07	− 2.08	0.224	0.017	0.210	0.018
1	0.92	10.05	0	0.478	0	0.481	0

Table 6 Mixed-wet reservoir carbonate (Alhammadi et al. 2020)

f_w	S_w	ΔP/kPa	P_c/kPa	Experimental k_{rw}	Experimental k_{ro}	Corrected k_{rw}	Corrected k_{ro}
0	0.185	4.43	− 0.15	0	0.841	0	0.821
0.15	0.305	8.14	− 0.39	0.030	0.389	0.031	0.415
0.3	0.390	11.93	− 0.50	0.040	0.219	0.037	0.238
0.5	0.578	31.33	− 0.59	0.026	0.060	0.039	0.070
0.7	0.623	27.77	− 0.64	0.040	0.040	0.043	0.049
0.85	0.674	26.13	− 0.61	0.052	0.021	0.052	0.023
0.95	0.699	20.06	− 0.63	0.076	0.009	0.073	0.012
1	0.822	3.45	0	0.464	0	0.466	0

Table 7 Water-wet reservoir sandstone (Gao et al. 2020)

f_w	S_w	ΔP/kPa	P_c/kPa	Experimental k_{rw}	Experimental k_{ro}	Corrected k_{rw}	Corrected k_{ro}
0	0.20	2.16	0	0	0.620	0	0.593
0.05	0.44	9.26	3.18	0.002	0.137	0.003	0.162
0.15	0.50	16.59	2.79	0.004	0.068	0.005	0.074
0.3	0.55	20.29	2.75	0.006	0.046	0.008	0.044
0.5	0.59	17.42	2.63	0.012	0.038	0.017	0.038
0.7	0.63	13.6	2.58	0.023	0.031	0.039	0.034
0.95	0.69	6.41	2.58	0.066	0.011	0.087	0.013
1	0.74	3.8	0	0.111	0	0.107	0

Table 8 Mixed-wet reservoir sandstone (Gao et al. 2020)

f_w	S_w	ΔP/kPa	P_c/kPa	Experimental k_{rw}	Experimental k_{ro}	Corrected k_{rw}	Corrected k_{ro}
0	0.17	1.99	0	0	0.677	0	0.646
0.05	0.37	9.6	1.82	0.002	0.135	0.002	0.224
0.15	0.45	32.11	0.77	0.003	0.036	0.002	0.066
0.3	0.50	42.29	− 0.74	0.004	0.022	0.004	0.033
0.5	0.54	51.21	− 0.75	0.005	0.013	0.007	0.016
0.7	0.62	53.88	− 0.80	0.006	0.007	0.021	0.008
0.95	0.66	18.01	− 0.85	0.022	0.004	0.049	0.006
1	0.82	2.19	0	0.191	0	0.215	0

Code Availability The code used for the analysis in this paper can be found at the link: https://github.com/ImperialCollegeLondon/relPermCorrection

Declarations

Conflict of interest The author declare that they have no conflict of interest.

References

Adler, P.M., Brenner, H.: Multiphase flow in porous media. Annu. Rev. Fluid Mech. **20**, 35–59 (1988)

Alhammadi, A.M., Gao, Y., Akai, T., Blunt, M.J., Bijeljic, B.: Pore-scale X-ray imaging with measurement of relative permeability, capillary pressure and oil recovery in a mixed-wet micro-porous carbonate reservoir rock. Fuel **268**, 117018 (2020)

Alizadeh, A., Piri, M.: The effect of saturation history on three-phase relative permeability: An experimental study. Water Resour. Res. **50**, 1636–1664 (2014)

Bear, J.: Dynamics of fluids in porous media. Courier corporation (1988)

Chen, A., Wood, A.: Rate effects on water-oil relative permeability. In: Proceedings of the international symposium of the society of core analysts, Edinburgh, Scotland, pp. 17–19 (2001)

Gao, Y., Lin, Q., Bijeljic, B., Blunt, M.J.: X-ray microtomography of intermittency in multiphase flow at steady state using a differential imaging method. Water Resour. Res. **53**, 10274–10292 (2017)

Gao, Y., Raeini, A.Q., Blunt, M.J., Bijeljic, B.: Pore occupancy, relative permeability and flow intermittency measurements using X-ray micro-tomography in a complex carbonate. Adv. Water Resour. **129**, 56–69 (2019)

Gao, Y., Raeini, A.Q., Selem, A.M., Bondino, I., Blunt, M.J., Bijeljic, B.: Pore-scale imaging with measurement of relative permeability and capillary pressure on the same reservoir sandstone sample under water-wet and mixed-wet conditions. Adv. Water Resour. **146**, 103786 (2020)

Gupta, R., Maloney, D.R.: Intercept method–a novel technique to correct steady-state relative permeability data for capillary end effects. SPE Reservoir Eval. Eng. **19**, 316–330 (2016)

Hassker, G., Brunner, E., Deahl, T.: The role of capillarity in oil production. Trans. AIME **155**, 155–174 (1944)

Herring, A.L., Harper, E.J., Andersson, L., Sheppard, A., Bay, B.K., Wildenschild, D.: Effect of fluid topology on residual nonwetting phase trapping: implications for geologic CO_2 sequestration. Adv. Water Resour. **62**, 47–58 (2013)

Huang, D.D., Honarpour, M.M.: Capillary end effects in coreflood calculations. J. Petrol. Sci. Eng. **19**, 103–117 (1998)

Jackson, S.J., Lin, Q., Krevor, S.: Representative elementary volumes, hysteresis, and heterogeneity in multiphase flow from the pore to continuum scale. Water Resour. Res. **56**, e2019WR026396 (2020)

Krevor, S.C., Pini, R., Li, B., Benson, S.M.: Capillary heterogeneity trapping of CO_2 in a sandstone rock at reservoir conditions. Geophys. Res. Lett (2011). https://doi.org/10.1029/2011GL048239

Lai, W., Brandt, H.: A pressure-history-matching method for determination of relative permeabilities. SPE Reserv. Eng. **3**(02), 651–661 (1988)

Leverett, M.: Capillary behavior in porous solids. Trans. AIME **142**, 152–169 (1941)

Li, H., Chen, S.N., Yang, D., Tontiwachwuthikul, P.: Estimation of relative permeability by assisted history matching using the ensemble Kalman filter method. J. Can. Pet. Technol. **51**(03), 205–214 (2012)

Lin, Q., Bijeljic, B., Pini, R., Blunt, M.J., Krevor, S.: Imaging and measurement of pore-scale interfacial curvature to determine capillary pressure simultaneously with relative permeability. Water Resour. Res. **54**, 7046–7060 (2018)

Lin, Q., Bijeljic, B., Berg, S., Pini, R., Blunt, M.J., Krevor, S.: Minimal surfaces in porous media: pore-scale imaging of multiphase flow in an altered-wettability Bentheimer sandstone. Phys. Rev. E **99**, 063105 (2019)

Lin, Q., Bijeljic, B., Foroughi, S., Berg, S., Blunt, M.J.: Pore-scale imaging of displacement patterns in an altered-wettability carbonate. Chem. Eng. Sci. **235**, 116464 (2021)

Øren, P.-E., Bakke, S., Arntzen, O.J.: Extending predictive capabilities to network models. SPE J. **3**, 324–336 (1998)

Osoba, J., Richardson, J., Kerver, J., Hafford, J., Blair, P.: Laboratory measurements of relative permeability. J. Petrol. Technol. **3**, 47–56 (1951)

Peksa, A.E., Wolf, K.-H.A., Zitha, P.L.: Bentheimer sandstone revisited for experimental purposes. Mar. Pet. Geol. **67**, 701–719 (2015)

Qadeer, S., Dehghani, K., Ogbe, D., Ostermann, R.: Correcting oil/water relative permeability data for capillary end effect in displacement experiments. In: Proceedings of the SPE california regional meeting, Long Beach, California, 23–25 March. Paper SPE 17423 (1988)

Qu, M.-L., Lu, S.-Y., Lin, Q., Foroughi, S., Yu, Z.-T., Blunt, M.J.: Characterization of Water Transport in Porous Building Materials Based on an Analytical Spontaneous Imbibition Model. Transport in Porous Media, pp. 1–16 (2022)

Raeini, A.Q., Giudici, L.M., Blunt, M.J., Bijeljic, B.: Generalized network modelling of two-phase flow in a water-wet and mixed-wet reservoir sandstone: uncertainty and validation with experimental data. Adv. Water Resour. **164**, 104194 (2022)

Storn, R.: On the usage of differential evolution for function optimization. In: Proceedings of north american fuzzy information processing. IEEE, pp. 519–523 (1996)

Virnovsky G, Skjaeveland S, Surdal J, Ingsoy P (1995) Steady-state relative permeability measurements corrected for capillary effects. In: SPE annual technical conference and exhibition. OnePetro

Wang, Y., Li, G., Reynolds, A.C.: Estimation of depths of fluid contacts and relative permeability curves by history matching using iterative ensemble-Kalman smoothers. SPE J. **15**(02), 509–525 (2010)

Zhang, Y., Li, H., Yang, D.: Simultaneous estimation of relative permeability and capillary pressure using ensemble-based history matching techniques. Transp. Porous Media **94**, 259–276 (2012)

Zou, S., Armstrong, R.T.: Multiphase flow under heterogeneous wettability conditions studied by special core analysis and pore-scale imaging. SPE J. **24**, 1234–1247 (2019)

Zou, S., Hussain, F., Arns, J.-Y., Guo, Z., Arns, C.H.: Computation of relative permeability from in-situ imaged fluid distributions at the pore scale. SPE J. **23**, 737–749 (2018)

Zou, S., Liu, Y., Cai, J., Armstrong, R.T.: Influence of capillarity on relative permeability in fractional flows. Water Resour Res **56**, e2020WR027624 (2020)